Influence of disorder on the transport and optical properties of a two-dimensional binary alloy

H. N. Nazareno
International Center of Condensed Matter Physics, Universidade de Brasília, P.O. Box 04513, 70910-900 Brasília - DF, Brazil

P. E. de Brito and E. S. Rodrigues
Universidade Católica de Brasília, Departamento de Física, Campus Águas Claras, 72030-070 Brasília - DF, Brazil

(Received 23 November 2002; revised manuscript received 31 March 2003; published 18 August 2003)

We address the issue of wave propagation in two-dimensional disordered systems, as well as analyze the role of disorder on transport and optical properties of a two-dimensional binary alloy. We present results regarding the propagating properties of wave packets in the alloy with an applied dc electric field. We also show the behavior of the specific heat as a function of temperature and the optical absorption coefficient for different alloy compositions and degrees of disorder.

DOI: 10.1103/PhysRevB.68.054204 PACS number(s): 72.15.Rn, 72.80.Ng, 73.23.−b

I. INTRODUCTION

The aim of this work is to analyze the influence of disorder on transport and optical properties of carriers in a two-dimensional binary alloy $a_x b_{1-x}$ of finite size, as well as the interplay between the degree of disorder and alloy composition. It is well established that there is no metal-insulator transition in disordered two-dimensional systems in the thermodynamic limit, in the absence of a magnetic field.[1] But the main subject of the present work is to analyze the behavior of mesoscopic systems such as the ones produced in the devices, so that our conclusions can not be assumed to hold in the thermodynamic limit.

Nevertheless, experiments done on clean samples of GaAs/AlGaAs heterostructures suggested that a metal-insulator transition could take place on a two-dimensional (2D) system.[2] Other groups, while studying the phase diagram of the quantum Hall effect in disordered Si metal oxide semiconductor field effect transistors (MOSFETs) and GaAs/AlGaAs heterostructures, arrived at similar conclusions.[3,4] On top of that, a systematic series of experiments recently done on MOSFETs compounds,[5–7] showed an *unusual* behavior, suggesting the existence of a metallic phase. They have observed that, for carrier densities above a critical value n_c, the resistivity decreases with decreasing temperature, a typical metallic behavior observed down to low temperatures. For an extensive account of the state of the art of the problem of localization in 2D disordered electronic systems see the work by Abrahams *et al.*[8]

We are aware that ours is a one-particle model. Nevertheless, there are situations in which even if the interaction between particles is relevant, a single particle description can give a clue to explain certain phenomena. We would like to refer to the detection of Bloch oscillations in superlattices,[9] a phenomenon predicted in the realm of one-particle physics. Another example being the detection of the famous Hofstadter butterfly spectrum for electrons in two-dimensions, under a magnetic field.[10] A noninteracting-electron model was recently introduced to describe a metal-insulator transition in two dimensions.[11]

In Sec. II we present the model Hamiltonian used to describe propagating properties in a 2D binary alloy with diagonal disorder under the action of a dc electric field, for different values of the order parameter and alloy composition. Following, we show the density of states (DOS) obtained, after solving the eigenvalue problem for each case in study. By applying the statistics of a Fermi gas, we obtain the specific heat as a function of temperature for the alloy. Finally, we present a model to obtain the behavior of the optical absorption coefficient of the alloy as a function of the incident photon frequency.

II. DYNAMICAL PROPERTIES

As stated above, we treat the problem of quantum percolation in a binary alloy $a_x b_{1-x}$, along the tight-binding model, with diagonal disorder, in a 2D underlying square lattice where the on-site energies ($\varepsilon_{n,m}=\varepsilon_a$ or ε_b) are randomly distributed under the action of an electric field $E_i (i=x,y)$. We expand the wave function in the Wannier representation

$$|\psi(t)\rangle = \sum_{n,m} f_{n,m}(t)|n,m\rangle \tag{1}$$

so that the time dependent Schrödinger equation is

$$i\frac{df_{n,m}}{d\tau} = (f_{n+1,m}+f_{n-1,m}+f_{n,m+1}+f_{n,m-1}) + (\epsilon_{n,m}+n\mathcal{E}_x+m\mathcal{E}_y)f_{n,m} \tag{2}$$

in terms of the dimensionless variables

$$\tau = \frac{Wt}{\hbar}, \quad \epsilon_{n,m}=\frac{\varepsilon_{n,m}}{W}, \quad \mathcal{E}_i=\frac{eaE_i}{W}, \tag{3}$$

where W is the hopping term considered to be constant and a is the lattice parameter. Taken as the initial condition a well localized particle at the origin of the lattice:

$$f_{n,m}(t=0)=\delta_{n,0}\delta_{m,0}. \tag{4}$$

In a previous work[12] it was shown that the set of equations can be cast in the matrix form

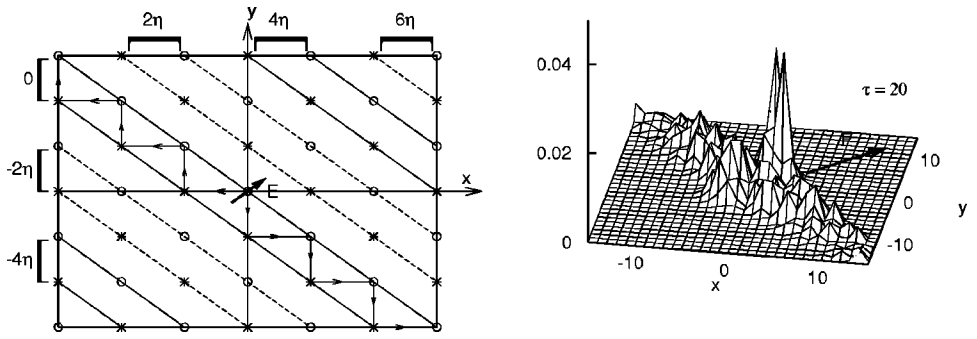

FIG. 1. The left figure indicates the occupation in the dimer structure of *a* sites (open circles) and *b* sites (asterisks). The brackets indicate the pairs of IFD lines with the same on-site energy. The example shown corresponds to the case $eEa/W=\eta$. Note the zigzag *easy* route for the packet. The right figure shows the packet at a particular time, making it evident that propagation occurs perpendicular to the applied field.

$$i\frac{d\mathbf{F}}{d\tau}=\mathbf{M}\mathbf{F} \tag{5}$$

where **M** is the dynamical matrix and the vector **F** is constructed from the Wannier amplitudes $f_{n,m}(\tau)$. To solve Eq. (5) we introduced a method that showed that the solution of the matrix equation can be cast as follows[13]:

$$\mathbf{F}(\tau)=\mathbf{R}^{t}\exp(-i\mathbf{D}\tau)\mathbf{R}\mathbf{F}(0), \tag{6}$$

where **D** is the diagonal form of the dynamical matrix **M**.

Since the lattice assumed in the simulations is finite of size $N=N_x\times N_y$, we chose it to be large enough in order to avoid boundary effects. As for the time limit taken in our calculation it was 10^{-11} sec, longer than any reasonable collision time in the sample, something that implies that we have to consider a lattice sufficiently large to eliminate undesirable boundary effects.

In order to describe the kind of propagation of an initially localized wave packet, we analyze the following: (i) The mean-square displacement (MSD) $\langle r^2\rangle$, which in units of the lattice parameter is given by

$$\langle r^2\rangle(t)=\sum_{n,m}|f_{n,m}(t)|^2(n^2+m^2). \tag{7}$$

(ii) We make three-dimensional plots of the wave packet taken at different times. It must be pointed out that this one-particle picture remains valid for sufficient long times such that the dephasing of the wave function due to interactions, with phonons for example, is not significant.

Given *x*, the concentration of *a*-atoms in the alloy, another crucial parameter that measures the degree of disorder in the present model is

$$\eta=\left|\frac{\varepsilon_a-\varepsilon_b}{W}\right|. \tag{8}$$

Our results will be characterized in terms of these two dimensionless parameters, since we are interested in studying the interplay between alloy composition and degree of disorder. The calculations proceeded as follows: Having chosen the concentration parameter *x*, we start at $t=0$ with the electron localized at a certain *a* site in the lattice. Clearly, when η is very small, hopping is favored *even* between sites occupied by atoms of different species. In such a case and independently of the concentration of the alloy, we have a *ballistic* propagation of the initially well localized wave packet: $\langle r^2\rangle=Ct^2$. On the other extreme, for sufficient large η, hopping between different atoms is strongly inhibited, and the wave remains *localized* in a definite region. For intermediate η values we can have several kinds of pictures characterized as superdiffusive, diffusive, or subdiffusive propagation.

In a previous work,[15] we presented a summary of the results obtained along the methods outlined above, by showing a phase diagram in the (x,η) plane, in which different types of propagation (localization) are indicated. We must point out that it is not only the strength of the disorder but also the dimensionality of the system that determines the kind of propagation (localization) of carriers. In 1D disordered *random* systems the situation was definitively established, that is, it is impossible for a carrier to propagate through them. Still in one dimension, we have exceptional situations that belong to the class of *deterministic* aperiodic structures such as Fibonacci, Thue-Morse, and Harper, where one can even obtain superdiffusive propagation.[16–18] But, as happens in this work, in a 2D system, due to the greater connectivity of the lattice, we expect a different behavior from the one-dimensional case.

A. Effect of a dc electric field

In our previous work[15] we did not include the presence of an electric field, with which we will deal now. A given random configuration results in a given site distribution, which in turn determines the route the wave follows as time progresses, as explained above. On the other hand, when the field is acting, sites that were degenerate in energy could no longer be so, and this inhibits propagation along these sites.

The inclusion of the electric field produces directions along which the additional potential energy is constant. We can call this effect *induced field degeneracy* (IFD). For a field $\mathbf{E}=E(1,\beta)$, the IFD lines satisfy the equation

$$y+\frac{x}{\beta}=cte,$$

which are *perpendicular* to the field. Sites along these lines tend to be degenerate due to the acting field. Consequently

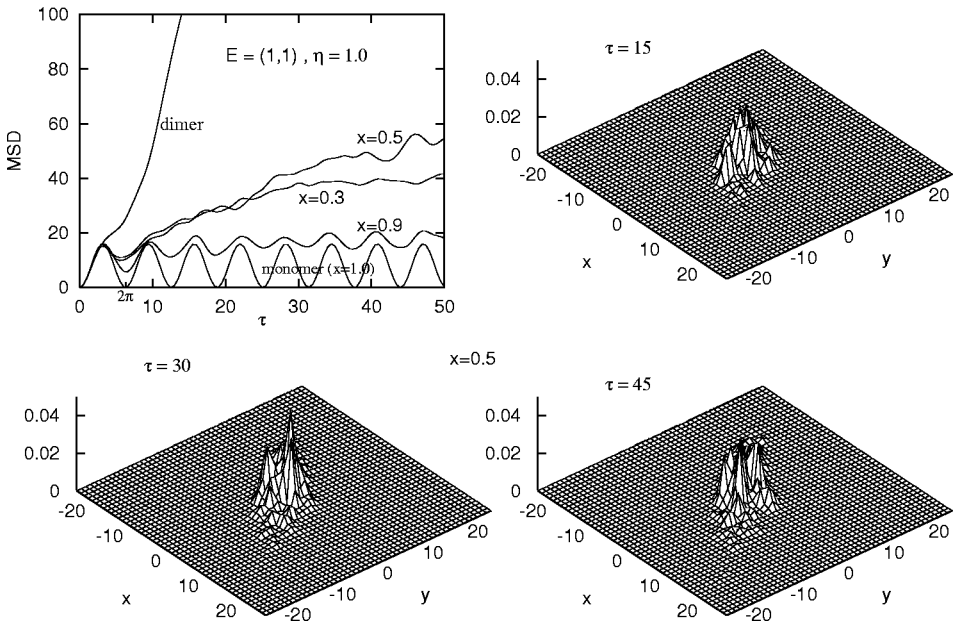

FIG. 2. For $\eta=1$ and an applied electric field $\mathbf{E}=E(1,1)$. The first figure shows the MSD for the concentrations $x=0.3$, 0.5, and 0.9 together with the monomer and dimer. The other figures show the wave packet evolution for $x=0.5$.

propagation is favored along these directions. See Fig. 1, where we illustrate the dimer situation.

Let us discuss different situations starting with the monomer case. It is well established that in such a system the action of a dc electric field produces Bloch oscillations.[12] Going to the dimer structure the behavior is dramatically different. In fact, let us consider the case of the field being applied along the diagonal $\mathbf{E}=E(1,1)$, for which the IFD lines are parallel to the secondary diagonal. The line passing through the origin contains sites with an on-site energy equal to zero (a type). The nearest neighboring (n.n.) lines contain sites with an on-site energy equal to $\eta \pm eEa/W$ (b-type), the n.n.n. lines contain sites with an on-site energy equal to $\pm 2eEa/W$, and so on. By tuning the field intensity we can cause the first two IFD lines to the right of the secondary diagonal to contain sites with the same on-site energy. In fact, taking, for instance, $eEa/W=\eta$, the first line contains sites with the same on-site energy as the second one, equal to 2η. Another two degenerate lines are the secondary diagonal and the first line to the left, with an on-site energy equal to zero. This explains why in the dimer case the wave propagates in the presence of an electric field, a different situation as compared with the monomer lattice. We can see in the present example that the direction of propagation is parallel to the secondary diagonal, i.e., *perpendicular* to the applied field. See Fig. 1.

It is interesting to analyze the effect of the application of a dc electric field, mainly in the case of small disorder ($\eta=1$), where we have ballistic propagation for all concentrations in the absence of the field.[15] By applying a field along the diagonal $\mathbf{E}=E(1,1)$ we note that the packet is localized in a very small region of the lattice. This is the phenomenon of *dynamic localization* as opposed to the case of Anderson localization,[14] caused by a sufficiently strong disorder. We note this dynamical effect in Fig. 2, where we show the wave packet for a concentration $x=0.5$, at three different times. The localization is evident, and the packet has a tendency to propagate along the direction *perpendicular* to the direction of the applied field, in agreement with the above explanation. For a concentration $x=0.9$ we observe an oscillation of the wave packet resembling the Bloch oscillation of the monomer, since, for these parameters, the alloy is close to the monomer structure. See the corresponding MSD shown in Fig. 2.

III. STATISTICAL PROPERTIES

In this section we are concerned with statistical properties such as the temperature dependence of the specific heat of our model alloy. In order to solve the stationary Schrödinger equation we expand the wave function in the Wannier representation

$$|\Psi(\mathbf{r})\rangle=\sum_{n,m} g_{n,m}|n,m\rangle, \tag{9}$$

which leads to the following set of equations for the amplitudes:

$$Eg_{n,m}=[g_{n+1,m}+g_{n-1,m}+g_{n,m+1}+g_{n,m-1}]+\epsilon_{n,m}g_{n,m}, \tag{10}$$

where the energies are in units of W. We have taken a lattice of $71\times71=5041$ sites which will produce that number of eigenfunctions and corresponding eigenvalues. Notice that now the Wannier amplitudes $g_{n,m}$ are time independent. We considered several alloy concentrations and different values of the crucial parameter η.

In order to check our programs, we calculated the spectrum of energies and the DOS for the ordered structures: the monomer and the periodic dimer for different values of η. In the latter cases one notices that the single band of the monomer splits into two sub-bands, with an energy gap equal to η. In Fig. 3 we show the DOSs for the monomer ($\eta=0$) and for the periodic dimers for $\eta=1$, 5, and 10; we note a reflection symmetry around the middle of the gap for the three

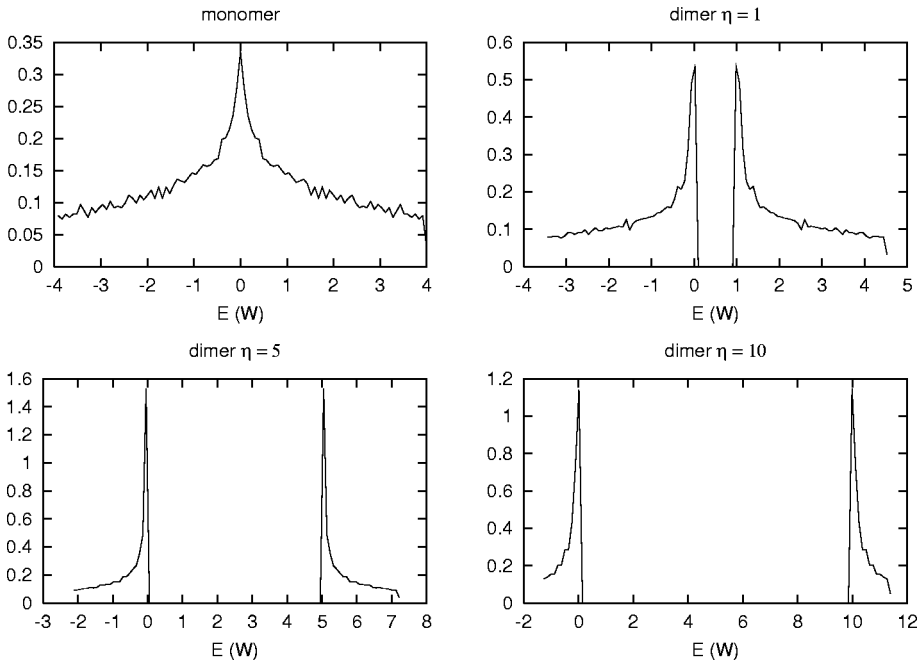

FIG. 3. The density of states (DOS) for the ordered structures: monomer (η=0) and dimers for η=1, 5, and 10, respectively.

dimers. Clearly, as we increase η, the bands get narrower, reaching the atomic limits when $|\varepsilon_a - \varepsilon_b| \gg gW$.

Performing the calculation for different disordered configurations, we noted, in the density of states, the appearance of states inside the gap region of the ordered structures; such states are localized ones. At the same time, the symmetry of the DOS presented in the ordered cases is absent in the alloy. First of all, in the five cases treated above for small disorder (η=1), the associated DOSs show no gap; in addition, as they resemble the DOSs of the monomer case since η is small. See Fig. 4, where we show the DOSs for $x=0.3$ and 0.5 and for the three cases η=1, 5, and 10. For intermediate disorder (η=5) the associated DOS shows the absence of a gap in the spectrum in any of the concentrations. We can compare the DOS corresponding to η=5 for the dimer with the alloy for a concentration $x=0.5$. In the alloy, the gap is completely closed, while the peaks which are present in the ordered structure are severely depleted; see Figs. 3 (η=5) and 4 ($x=0.5$ and η=5). For large disorder (η=10), a common feature for all the cases is the presence of gaps in the spectra, due to the great η. We can again compare the obtained DOSs for $x=0.5$ and η=10 shown in Fig. 4 with the corresponding DOS in the ordered dimer shown in Fig. 3. Similar to the case of intermediate disorder, the peaks in the

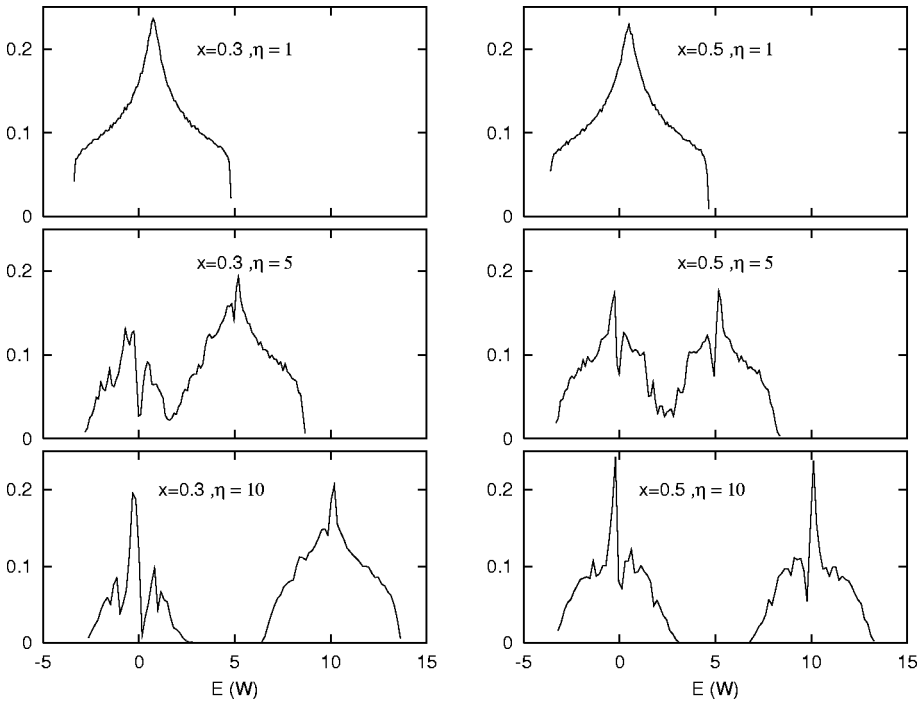

FIG. 4. The DOSs for $x=0.3$ and 0.5 and η=1, 5, and 10.

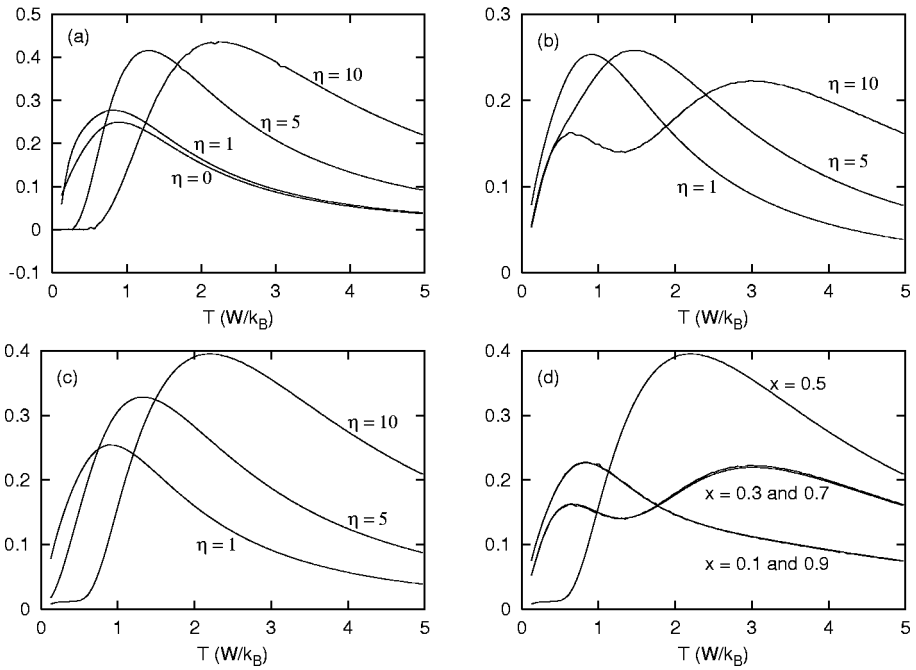

FIG. 5. The specific heat as a function of temperature. (a) Specific heat for the four ordered cases. (b) Specific heat for concentration $x=0.3$ and $\eta=1$, 5, and 10. (c) Specific heat for $x=0.5$ and $\eta=1$, 5, and 10. (d) Specific heat for $\eta=10$ and concentrations $x=0.1$, 0.3, 0.5, 0.7, and 0.9. The temperature units are W/k_B, where k_B is the Boltzmann constant.

ordered structure are depleted in the alloy. The difference is that in this case of large η, the states that appear in the gap region cannot fill it completely. It is interesting to analyze a less symmetric case, namely, one with $x=0.3$ and $\eta=10$ (see Fig. 4). Since x is the concentration of a atoms, the corresponding subband is narrower than the b subband. Still, in this case, the DOS presents an appreciable gap. If we consider the same concentration of a atoms but now take a smaller $\eta=5$, we notice that there is no gap.

Specific heat

Having solved the Schrödinger equation we must apply the recipes of statistical mechanics to obtain the internal energy and the specific heat. Considering a number of carriers that can fill $N/2$ levels (a subband) we set the condition

$$\frac{N}{2}=\sum_k \left[e^{\beta(E_k-\mu)}+1\right]^{-1} \tag{11}$$

from which the chemical potential as a function of temperature is obtained. After this we evaluate the internal energy $U(T)$:

$$U(T)=\sum_k \frac{E_k}{e^{\beta(E_k-\mu)}+1}. \tag{12}$$

After this step is completed we are in a position to evaluate the specific heat:

$$C_v(T)=\frac{\partial U}{\partial T}. \tag{13}$$

We now present the results corresponding to the specific heat as a function of temperature, for different values of the parameters x and η:

In Fig. 5(a) we show the specific heat curves for the four ordered cases, the monomer and the three dimers corresponding to $\eta=1$, 5, and 10. Notice that the position and intensity of the peak, in the specific heat, are increasing with temperature as, the gap η, in the DOS, increases. Now we discuss the results obtained for an alloy corresponding to different values of x and η. Fixing the concentration we varied the parameter η and found a definite trend in the behavior of the specific heat as a function of temperature. We first, consider the cases $x=0.3$ and $\eta=1$, 5, and 10. In the two former cases we noticed that the specific heat curves showed a single peak, while in the latter case two peaks were present [see Fig. 5(b)]. Going back to the DOS associated with these cases, we see (in Fig. 4) that we obtained a gap in the spectrum for $\eta=10$, while for $\eta=5$ and 1 the gap is closed. This is due to the presence of the two asymmetric subbands in the case of $\eta=10$, the one responsible for the appearance of the two peaks in the specific heat. In Fig. 5(c) we show the specific heat for $x=0.5$ and $\eta=1$, 5, and 10. Note that there is a single peak for all three cases, while for the two smaller values of η, no gap is present in the DOS, in addition for $\eta=10$ there is a gap in the spectrum, which showed two *symmetric* subbands.

In Fig. 5(d) we show the case $\eta=10$ for five concentrations. Because of symmetry, the curves corresponding to $x=0.1$ and 0.9 coincide; the same occurs for concentrations $x=0.3$ and 0.7. If we compare this with the ordered cases in which the specific heat has a single peak irrespective of the magnitude of the gap, in the case of the alloy the presence of two peaks is due to both conditions: the existence of the gap *and* the asymmetry in the spectrum. Note that, in the ordered cases, the DOS presents a reflection symmetry, that is absent in the alloy. The asymmetry in the DOS is greater for a concentration $x\approx 0.25$, while the two peaks are of the same intensity and more pronounced than for other concentrations. In all cases the specific heat goes to zero as $T\to\infty$, since the spectrum is bounded.

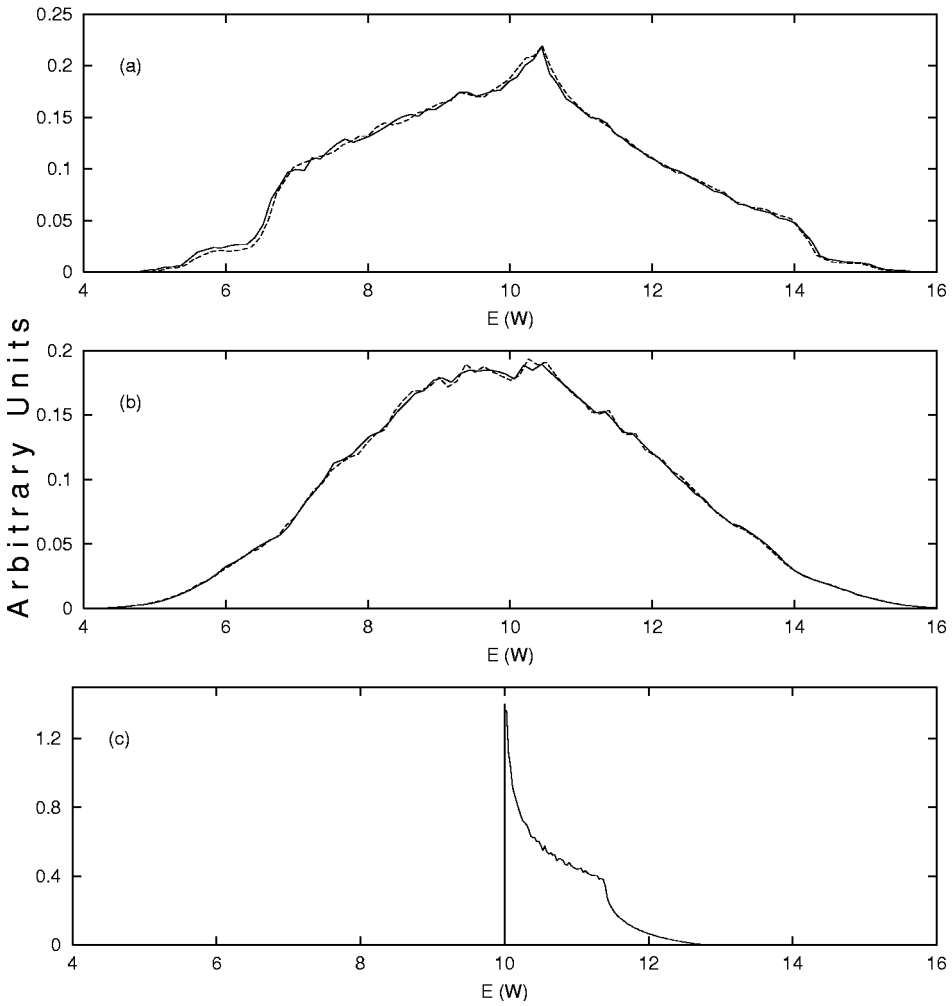

FIG. 6. The optical absorption coefficient in arbitrary units as a function of the incident photon energy. (a) The absorption coefficient for concentrations $x=0.1$ (continuous line) and $x=0.9$ (dashed line). (b) The absorption coefficient for concentrations $x=0.3$ (continuous line) and $x=0.7$ (dashed line). (c) The absorption coefficient for the dimer corresponding to $\eta=10$.

IV. OPTICAL ABSORPTION

For the cases shown above, in which, due to a large η, the spectrum shows a gap, we can study the optical absorption due to interband transitions. In fact, once the energy spectrum and the DOS of the alloy are determined, we can calculate the optical absorption coefficient as a function of the incident photon frequency ω, due to transitions between bands, which we shall call a and b. Considering vertical transitions, one can write the absorption coefficient in the compact form

$$\alpha(\omega)=\frac{\mathcal{M}}{\omega}\times J_{ab}(\hbar\omega), \tag{14}$$

where $J_{ab}(\omega)$ is the joint density of states (JDOS) and $\mathcal{M}$ is proportional to the matrix element of the perturbation between initial and final states. In the Appendix we show the steps that lead to this expression for the absorption coefficient.[19,20]

We shall first present the results for the ordered dimer where the density of states is a maximum one for the top of the ''valence'' band a and the bottom of the ''conduction'' band b. As a consequence, the JDOS presents a maximum at an energy equal to the gap. In this way, the band-to-band transitions spectrum peaks at $\hbar\omega=E_{gap}$. Moreover, it presents a shoulder for a frequency for which $(\varepsilon_b-\varepsilon_a)/\hbar$ is a maximum one, because it is a critical point or a Van Hove singularity.[21,22]

Following this, we consider the alloy case for different alloy compositions and for a fixed value of the disorder parameter η. First of all, as stated above, in the case of a disordered system the gap between bands is reduced, which means that the absorption threshold occurs at a lower frequency as compared with the ordered case. At the same time we note that the peak in the spectrum appears at an energy (frequency) close to, but a little larger than, the energy of the gap of the ordered case (see Fig. 6). This behavior is common to all alloy compositions, as can be noticed in Figs. 6(a)–6(c) where we show the absorption coefficient for $\eta=10$ and concentrations $x=0.1$, 0.3, 0.7, and 0.9 and for the corresponding dimer. The absorption curves for the two concentrations $x=0.1$ and 0.9 coincide because of the structure of the corresponding DOS; the same happens with the cases $x=0.3$ and 0.7. Note that the peak of the absorption coefficient of the dimer is much greater than the ones in the alloy cases.

V. CONCLUSIONS

In the present work we analyzed the propagation properties of carriers in a 2D binary alloy a_xb_{1-x} along the tight-

binding model with diagonal disorder under the action of a dc electric field, and presented the results of the specific heat as a function of temperature as well as the optical absorption coefficient for several compositions (x) and intensities of the disorder (η). In a previous work[15] we presented, through a phase diagram in the (x,η) plane, the different kinds of behavior concerning the propagation properties of wave packets in the binary alloy, without the presence of an electric field.

The inclusion of a dc electric field radically changes the behavior observed in the absence of the field. In fact, as previously shown, its effect is more evident in the case of small disorder, where ballistic propagation is obtained in the field free case; however once it is included, a strong localization is observed. As explained above, the field breaks the degeneracy of sites of the same kind, inhibiting propagation along them. We also discussed the effect of the presence of a field in the case of a dimer structure, where we explained why, by properly tuning the electric field, it is possible to create pair of lines perpendicular to the field, that contain degenerate sites which in turn produces propagation along them. This is the effect due to the presence of the field, that we called *induced field degeneracy*.

We also presented the density of states for different alloy compositions and different degrees of disorder. When we compared the results for the alloy with ordered 2D structures for several values of η, we observed, in the gap region of the ordered dimers, the appearance of states in the alloy case. If the degree of disorder is sufficiently large, there is still a gap in the alloy spectrum, although smaller than in the corresponding ordered case. For small to moderate disorder, the gap is closed by the presence of localized states. In other words, for large η the spectrum is characterized by two subbands separated by a gap, while for smaller values of η no gap is present in the DOS. This has as the immediate consequence that, for an alloy with large η and a concentration such that its corresponding DOS is asymmetric, the specific heat as a function of temperature shows two peaks. In the absence of a gap in the spectrum (small to moderate η) the curve shows a single peak.

Finally, we evaluated the optical absorption coefficient of the alloy by considering interband transitions for the cases in which, due to large values of the disorder parameter η, there is a gap in the spectrum. The maximum in the absorption curve occurs for an energy a bit larger than the energy gap in the spectrum of the ordered dimer.

APPENDIX

To obtain Eq. (14) we proceed as follows. We take the interaction between electrons and the radiation field of frequency ω, in the linear approximation in the vector potential which satisfies the Lorentz gauge $\nabla\cdot\mathbf{A}=0$,

$$H_{int}=\frac{e}{mc}[\mathbf{A}(\mathbf{x},t)\cdot\mathbf{p}]. \tag{A1}$$

We apply the Fermi golden rule to calculate the transition probability per unit time between an initial state $|i\rangle$ with energy ε_i to a final state $|f\rangle$ with energy ε_f:

$$P_{if}(\omega)=\frac{1}{\hbar}|\langle f|H_{int}|i\rangle|^2\delta(\varepsilon_f-\varepsilon_i-\hbar\omega). \tag{A2}$$

To get the total number of transitions per unit time we must perform a sum over all states in both bands that are separated in energy by the photon incident energy $\hbar\omega$:

$$W(\omega)=\sum_{i\to f}P_{if}(\omega). \tag{A3}$$

The absorption coefficient α is the ratio between the energy absorbed in the unit time and the energy flux $u(c/n)$, where u is the density of energy of the electromagnetic field and n is the refraction index,

$$\alpha=\frac{\hbar\omega W(\omega)}{u(c/n)} \tag{A4}$$

where the average energy density u in the medium is given by

$$u=C\frac{\omega^2}{(c/n)^2} \tag{A5}$$

If we consider the matrix elements of Eq. (A2) as a constant, we can extract the joint density of states to obtain Eq. (14) for the absorption coefficient.

[1] E. Abrahams, P.W. Anderson, D.C. Licciardello, and T.V. Ramakrishnan, Phys. Rev. Lett. **42**, 673 (1979).

[2] A. Gold, Phys. Rev. B **44**, 8818 (1991).

[3] V.M. Pudalov, M. D'Íorio, S.V. Kravchenko, and J.W. Campbell, Phys. Rev. Lett. **70**, 1866 (1993).

[4] A.A. Shashkin, G.V. Kravchenko, and V.T. Dolgopolov, Pis'ma Zh. Éksp. Teor. Fiz. **58**, 215 (1993) [JETP Lett. **58**, 220 (1993)].

[5] S.V. Kravchenko, Whitney E. Mason, G.E. Bowker, J.E. Furneaux, V.M. Pudalov, and M. DIorio, Phys. Rev. B **51**, 7038 (1995).

[6] V.M. Pudalov, G. Brunthaler, A. Prinz, and G. Bauer, Pis'ma Zh. Éksp. Teor. Fiz. **65**, 887 (1997) [JETP Lett. **65**, 932 (1997)].

[7] S.V. Kravchenko, D. Simonian, K. Mertes, M.P. Sarachik, and T.M. Klapwijk, Phys. Rev. B **59**, R12740 (1999).

[8] Elihu Abrahams, Sergey V. Kravchenko, and Myriam P. Sarachik, Rev. Mod. Phys. **73**, 251 (2001).

[9] Christian Waschke, Hartmut G. Roskos, Ralf Schwedler, Karl Leo, Heinrich Kurz, and Klaus Kohler, Phys. Rev. Lett. **70**, 3319 (1993).

[10] C. Albrecht, J.H. Smet, K. von Klitzing, D. Weiss, V. Umansky, and H. Schweizer, Phys. Rev. Lett. **86**, 147 (2001).

[11] Yigal Meir, Phys. Rev. Lett. **83**, 3506 (1999); Phys. Rev. B **61**, 16470 (2000).

[12] H.N. Nazareno and Y. Lepine, Phys. Rev. B **55**, 6661 (1997).

[13] H.N. Nazareno, C.A.A. da Silva, and P.E. de Brito, Phys. Rev. B **50**, 4503 (1994).
[14] P.W. Anderson, Phys. Rev. **109**, 1492 (1958).
[15] H.N. Nazareno, P.E. de Brito, and E.S. Rodrigues, Phys. Rev. B **66**, 012205 (2002).
[16] P.E. de Brito, C.A.A. da Silva, and H.N. Nazareno, Phys. Rev. B **51**, 6096 (1995).
[17] H.N. Nazareno, P.E. de Brito, and C.A.A. da Silva, Phys. Rev. B **51**, 864 (1995).
[18] P.E. de Brito, Jorge A. Gonzalez, and H.N. Nazareno, Phys. Rev. B **54**, 12820 (1996).
[19] F. Bassani and G. Pastori Parravicini, in *Electronic States and Optical Transitions in Solids*, edited by R. A. Ballinger (Pergamon Press, Oxford, 1975).
[20] H.N. Nazareno and M.A. Amato, J. Phys. C **15**, 2165 (1982).
[21] J.C. Phillips, Phys. Rev. **104**, 1263 (1956).
[22] L. Van Hove, Phys. Rev. **89**, 1189 (1953).